

Dream to Drive: Model-Based Vehicle Control Using Analytic World Models

Asen Nachkov¹ Danda Pani Paudel¹ Jan-Nico Zaech¹ Davide Scaramuzza² Luc Van Gool^{1,3}

Abstract—Differentiable simulators have recently shown great promise for training autonomous vehicle controllers. Being able to backpropagate through them, they can be placed into an end-to-end training loop where their known dynamics turn into useful priors for the policy to learn, removing the typical black box assumption of the environment. So far, these systems have only been used to train policies. However, this is not the end of the story in terms of what they can offer. Here, for the first time, we use them to train world models. Specifically, we present three new task setups that allow us to learn next state predictors, optimal planners, and optimal inverse states. Unlike analytic policy gradients (APG), which requires the gradient of the next simulator state with respect to the current actions, our proposed setups rely on the gradient of the next state with respect to the current state. We call this approach Analytic World Models (AWMs) and showcase its applications, including how to use it for planning in the Waymax simulator. Apart from pushing the limits of what is possible with such simulators, we offer an improved training recipe that increases performance on the large-scale Waymo Open Motion dataset by up to 12% compared to baselines at essentially no additional cost.

I. INTRODUCTION

Differentiable simulation has emerged as a powerful tool to train controllers and predictors across different domains like physics [22, 55, 31], graphics [26, 24, 65], and robotics [23, 8, 4, 50]. Within the field of autonomous vehicles (AVs), it was recently shown that differentiable motion dynamics can serve as a useful stepping stone for training robust and realistic vehicle policies [39]. The framework is straightforward and bears similarity to backpropagation through time – it involves rolling out a trajectory and supervising it with a ground-truth (GT) expert one. The process is sample-efficient because the gradients of the dynamics automatically guide the policy toward optimality and there is no search involved, unlike when the environment is treated as black box.

Yet, this has only been explored for single policies, which are *reactive* [53] in their nature – at test-time they simply associate an action with each observation without providing any guarantee for their expected performance. Unlike them, model-based methods use planning at test time [44], which *guarantees* to maximize the estimated reward. They are considered more interpretable compared to model-free methods, due to the simulated world dynamics, and more amenable to conditioning, which makes them potentially safer [42]. They are also sample-efficient due to the self-supervised training [5].

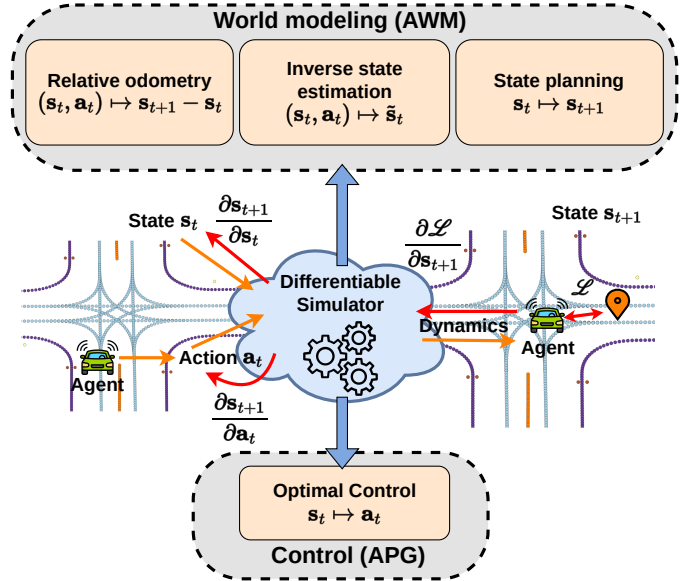


Fig. 1: **Differentiable simulation allows for a variety of learning tasks.** Previously, differentiable simulators have been used to train controllers using analytic policy gradients (bottom). Here, we propose to use them for learning relative odometry, state planning, and inverse state estimation (top).

Consequently, the ability to plan at test time is a compelling requirement towards accurate and safe autonomous driving.

An open question is *whether model-based methods can be trained and utilized in a differentiable environment*, and what would be the benefits of doing so. We tackle this question here. Naturally, planning requires learning a world model, but the concept of a world model is rather nuanced, as there are different ways to understand the effect of one’s own actions. Fig. 1 shows our approach, which uses the differentiability of the simulator to formulate three novel tasks related to world modeling. First, the effect of an agent’s action could be understood as the difference between the agent’s next state and its current state. If a vehicle’s state consists of its position, yaw, and velocity, then this setup has an odometric interpretation. Second, an agent could predict not an action, but a *desired* next state to visit, which is a form of state planning. Third, we can ask “*Given an action in a particular state, what should the state be so that this action is optimal?*”, which is another form of world modeling but also an inverse problem.

Thus, we are motivated to understand the kinds of tasks solvable in a differentiable simulator for vehicle motion. Policy learning with differentiable simulation is called Analytic Policy Gradients (APG). Similarly, we call the proposed approach

¹INSAIT, Sofia University “St. Kliment Ohridski”, Sofia, Bulgaria

²University of Zurich, Zurich, Switzerland

³ETH Zurich, Zurich, Switzerland

Analytic World Models (AWMs). It is intuitive, yet distinct from APG because APG requires the gradients of the next state with respect to the current actions, while AWM requires the gradients of the next state with respect to the current state.

The benefit of using a differentiable environment for solving these tasks is twofold. First, by not assuming black box dynamics, one can avoid *searching* for the solution, which improves sample efficiency. Second, when the simulator is put into an end-to-end training loop, the differentiable dynamics serve to better condition the predictions, leading to more physically-consistent representations, as evidenced from other works. This happens because the gradients of the dynamics get mixed together with the gradients of the predictors. More generally, similar to how differentiable rendering [26, 24] allows us to solve inverse graphics tasks, we believe that differentiable simulation allows us to solve new inverse dynamics tasks.

Having established the world modeling tasks, we use them for planning at test time. Specifically, we formulate a method based on model-predictive control (MPC), which allows the agent to autoregressively imagine future trajectories and apply the proposed world modeling predictors on their imagined states. Thus, the agent can efficiently compose these predictors in time. Note that this requires another world modeling predictor – one that predicts the next state latent sensory features from the current ones. This is the de facto standard world model [15]. Its necessity results only from the architectural design, to drive the autoregressive generation. Contrary to it, the predictions from our three proposed tasks are interpretable and meaningful, and represent a step towards the goal of having robust accurate planning for driving.

We use Waymax [14] as our simulator of choice, due to it being fully differentiable and data-driven. The scenarios are instantiated from the large-scale Waymo Open Motion Dataset (WOMD) [11] and are realistic in terms of roadgraph layouts and traffic actors. Apart from establishing new ways of using the differentiable simulator, we offer an improved training recipe over the previous APG work, resulting in up to 12% improvement in the average displacement error on WOMD while using an equal or smaller amount of compute. This improvement results from shorter training to limit any possible overfitting to the training trajectories and a regularization term that encourages the entropy of the policy. Additionally, we substitute the non-differentiable computation for collision detection in Waymax with a differentiable approximation based on Gaussian overlap. This allows us to differentiate not only through the dynamics, but also through the agent poses themselves. The learning signal from this overlap is sparse, yet conceptually useful to make the training setup complete.

Contributions. Our contributions are the following:

- In Sec. III-B to III-D we present three world modeling tasks, solvable within a differentiable simulator – relative odometry, state planning, and inverse state estimation.
- In Sec. III-E and III-F we implement predictors for these tasks and present a planning agent that uses them.
- We train and evaluate our proposed setups in the Waymax simulator [14], and further study them in multiple

settings and conditions. In the process, we introduce technical modifications, such as differentiable overlap, for improved training relative to the baseline APG method.

II. RELATED WORK

Differentiable simulation. The most relevant work is Analytic Policy Gradients (APG) applied for vehicle motion [39]. It trains near-optimal policies in a supervised manner, relying on the differentiability of the Waymax simulator [14]. The authors present a recurrent model that selects actions autoregressively from the observed agent locations, nearest roadgraph points, traffic lights, and goal heading. At training time the model learns to select those actions that would bring the simulated trajectory as close as possible to the log-trajectory. By adopting a GRU architecture, the derivatives of the dynamics from each timestep mix with those of the RNN hidden state and propagate backwards until the start of the trajectory. Compared to this APG model, we aim to introduce planning in the differentiable environment.

More generally, differentiable simulators have grown in popularity because they allow one to solve ill-posed inverse problems related to the dynamics. As examples, an object’s physical parameters like mass, friction, and elasticity could be estimated directly from videos and real-world experiments [7, 38, 13], or simulations of soft material cutting could enable precise calibration and policy learning [21]. Simulations can be parallelized across accelerators to enable efficient scaling of problem and experiment sizes [61, 33, 12].

Within the field of robotics, differentiable simulation is used extensively, especially for training robotic policies in physically-realistic settings [41, 32, 54, 45, 22]. The focus has often been on object manipulation [29, 60, 62, 30] which requires having differentiable contact models for detecting collisions – something lacking in the Waymax dynamics. Analytic policy gradients (APG) has been used to train policies for trajectory tracking and navigation in quadrotors and fixed-wing drones [58], quadruped locomotion [51], and for quadrotor control from visual features [20].

Driving simulators like CARLA [10, 34] have been used in autonomous driving [6, 64], with less focus on differentiable ones [27]. Some are differentiable but lack expert actions [27], others are lacking acceleration support, which is crucial for large scale training [52, 28, 57]. Waymax [14] was introduced recently as a data-driven simulator for vehicle motion. It represents vehicles as 2D boxes and supports acceleration.

Planning. Planning using world models [47, 15, 35] is a classic topic with two main approaches: model-predictive control (MPC) [2] and Dyna-style imagination [53]. With MPC [1, 46, 25], one starts with a random policy from which actions are sampled and evaluated. Then, the policy is repeatedly refit on only the best trajectories, from which new trajectories are sampled. Eventually, an aggregated action from the best trajectories is selected and executed. Being closed-loop, this strategy is repeated at every timestep. Dyna-style planning relies on the agent simulating entire trajectories and using them to update its policy [17, 18, 19]. Compared to

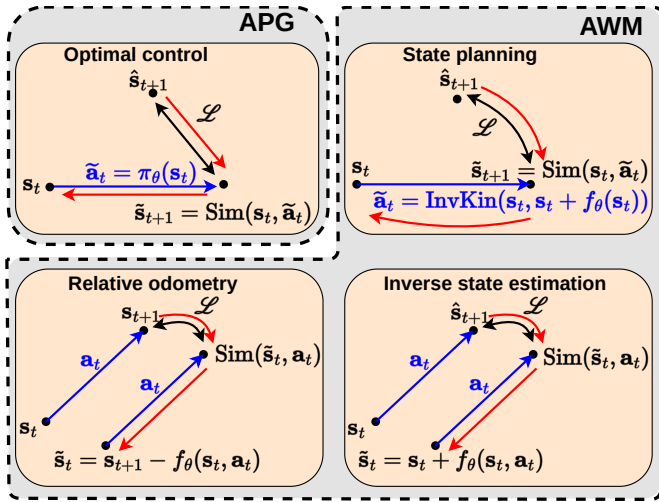


Fig. 2: **Detailed APG and AWM task formulations.** Black dots are states, blue arrows are actions, red arrows are gradients. Correspondence to sections is as follows: optimal control – Sec. III-A; state planning – Sec. III-C; relative odometry – Sec. III-B; inverse state estimation – Sec. III-D.

MPC which is computationally heavy at test-time, Dyna-like algorithms are lightweights and rely on the reactive policy being trained on both real and imagined transitions.

III. METHOD

In this section we introduce different task setups showcasing the usage of a differentiable simulator and the benefits it offers. Subsequently, in Sec. III-E and III-F, we introduce the agent architecture and the planning at test time.

Notation. In all that follows we represent the current simulator state with s_t , the current action with \mathbf{a}_t , the log (expert) state with \hat{s}_t , the log action with $\hat{\mathbf{a}}_t$. The simulator is a function $\text{Sim} : \mathcal{S} \times \mathcal{A} \rightarrow \mathcal{S}$, with $\text{Sim}(s_t, \mathbf{a}_t) \mapsto s_{t+1}$, where the set of all states is \mathcal{S} and that of the actions \mathcal{A} .

A. Preliminaries – APG

It is shown in [39] that a differentiable simulator can turn the search problem of optimal policy learning into a supervised one. Here the policy π_θ produces an action \mathbf{a}_t from the current state, which is executed in the environment to obtain the next state s_{t+1} . Comparing it to the log-trajectory \hat{s}_{t+1} produces a loss, whose gradient is backpropagated through the simulator and back to the policy:

$$\min_{\theta} \left\| \text{Sim}(s_t, \pi_\theta(s_t)) - \hat{s}_{t+1} \right\|_2^2. \quad (1)$$

The key gradient here is that of the next state with respect to the current agent actions $\frac{\partial s_{t+1}}{\partial \mathbf{a}_t}$. The loss is minimized whenever the policy outputs an action equal to the inverse kinematics $\text{InvKin}(s_t, \hat{s}_{t+1})$. To obtain similar supervision without access to a differentiable simulator, one would need to supervise the policy with the inverse kinematic actions, which are unavailable if the environment is considered a black box. Hence, this is an example of an inverse dynamics problem

that is not efficiently solvable without access to a known environment, in this case to provide inverse kinematics.

B. Relative odometry

In this simple setting a world model $f_\theta : \mathcal{S} \times \mathcal{A} \rightarrow \mathcal{S}$ predicts the next state s_{t+1} from the current state-action pair (s_t, \mathbf{a}_t) . Here, a differentiable simulator is not needed to learn a good predictor. One can obtain $(s_t, \mathbf{a}_t, s_{t+1})$ tuples simply by rolling out a random policy and then supervising the predictions with the next state s_{t+1} . Nonetheless, we provide a formulation for bringing the simulator into the training loop of this task:

$$\min_{\theta} \left\| \text{Sim}^{-1}(f_\theta(s_t, \mathbf{a}_t), \mathbf{a}_t) - s_t \right\|_2^2. \quad (2)$$

Here, the world model f_θ takes (s_t, \mathbf{a}_t) and returns a next-state estimate \tilde{s}_{t+1} . We then feed it into an inverse simulator Sim^{-1} which is a function with the property that $\text{Sim}^{-1}(\text{Sim}(s_t, \mathbf{a}_t), \mathbf{a}_t) = s_t$. This output is compared with the current s_t . The loss is minimized when f_θ predicts exactly s_{t+1} , thus becoming a predictor of the next state.

We implement the inverse simulator for the bicycle dynamics in Waymax [14], however observe that it is problematic in the following sense. The velocities v_x and v_y are tied to the yaw angle of the agent through the relationship $v_x = v \cos \phi$ and $v_y = v \sin \phi$, where ϕ is the yaw angle and v is the current speed. However, at the first simulation step, due to the WOM dataset [11] being collected with noisy estimates of the agent state parameters, the relationships between v_x , v_y , and ϕ do not hold. Thus, the inverse simulator produces incorrect results for the first timestep.

For this reason, we provide another formulation for the problem that only requires access to a forward simulator:

$$\min_{\theta} \left\| \text{Sim}(s_{t+1} - f_\theta(s_t, \mathbf{a}_t), \mathbf{a}_t) - s_{t+1} \right\|_2^2. \quad (3)$$

Here, f_θ predicts the relative state difference that executing \mathbf{a}_t will bring to the agent. One can verify that the loss is minimized if and only if the prediction is equal to $s_{t+1} - s_t$. This can still be interpreted as a world model where f_θ learns to estimate how an action would change its relative state. Since the time-varying elements of the agent state consist of (x, y, v_x, v_y, ϕ) , this world model has a clear relative odometric interpretation. Learning such a predictor without a differentiable simulator will prevent the gradients of the environment dynamics from mixing with those of the network.

Inverse dynamics and inverse kinematics. Given a tuple $(s_t, \mathbf{a}_t, s_{t+1})$, one can learn inverse dynamics $(s_{t+1}, \mathbf{a}_t) \mapsto s_t$ and inverse kinematics $(s_t, s_{t+1}) \mapsto \mathbf{a}_t$ without a differentiable simulator, which is useful for exploration [43]. Formulations that involve the simulator are also possible. We do not list them here because they are similar to Eqn. 3.

C. Optimal planners

We call the network $f_\theta : \mathcal{S} \rightarrow \mathcal{S}$ with $s_t \mapsto s_{t+1}$ a planner because it plans out the next state to visit from the current one. Unlike a policy, which selects an action without explicitly knowing the next state, the planner does not execute

any actions. Hence, until an action is executed, its output is inconsequential. We consider the problem of learning an optimal planner. With a differentiable simulator, as long as we have access to the inverse kinematics, we can formulate the optimisation as:

$$\min_{\theta} \left\| \text{Sim} \left(\mathbf{s}_t, \text{InvKin}(\mathbf{s}_t, \mathbf{s}_t + f_{\theta}(\mathbf{s}_t)) \right) - \hat{\mathbf{s}}_{t+1} \right\|_2^2. \quad (4)$$

Here, f_{θ} predicts the next state to visit as an offset to the current one. The action that reaches it is obtained using the inverse kinematics. After executing the action we directly supervise with the optimal next state. The gradient of the loss goes through the simulator, then through the inverse kinematics, and finally through the state planner network. Note that with a black box environment we can still supervise the planner directly with $\hat{\mathbf{s}}_{t+1}$, but a black box does not provide any inverse kinematics, hence there is no way to perform trajectory rollouts, unless with a separate behavioral policy.

D. Inverse optimal state estimation

We now consider the following task "Given $(\mathbf{s}_t, \mathbf{a}_t)$, find an alternative state for the current timestep t where taking action \mathbf{a}_t will lead to an optimal next state $\hat{\mathbf{s}}_{t+1}$ ". We formulate the problem as

$$\min_{\theta} \left\| \text{Sim}(\mathbf{s}_t + f_{\theta}(\mathbf{s}_t, \mathbf{a}_t), \mathbf{a}_t) - \hat{\mathbf{s}}_{t+1} \right\|_2^2. \quad (5)$$

Here f_{θ} needs to estimate the effect of the action \mathbf{a}_t and predict a new state $\tilde{\mathbf{s}}_t$, relatively to the current state \mathbf{s}_t , such that after executing \mathbf{a}_t in it, the agent reaches $\hat{\mathbf{s}}_{t+1}$. The loss is minimized if f_{θ} predicts $\tilde{\mathbf{s}}_t - \mathbf{s}_t$. The key gradient, as in Eqns. 2, 3, and 4, is that of the next state with respect to the current state. Given the design of the Waymax simulator [14], these gradients are readily-available.

Consider solving this task with a black box environment. To do so, one would need to supervise the prediction $f_{\theta}(\mathbf{s}_t, \mathbf{a}_t)$ with the state $\tilde{\mathbf{s}}_t - \mathbf{s}_t$, with $\tilde{\mathbf{s}}_t$ being unknown. By definition $\tilde{\mathbf{s}}_t = \text{Sim}^{-1}(\hat{\mathbf{s}}_{t+1}, \mathbf{a}_t)$, which is unobtainable since under a black box environment assumption, Sim^{-1} is unavailable. Hence, this is another inverse problem which is not solvable unless we are given more information about the environment, here specifically its inverse function.

The utility of this task is in providing a "confidence" measure to an action. If the prediction of f_{θ} is close to $\mathbf{0}$, then the agent is relatively certain that the action \mathbf{a}_t is close to optimal. Likewise, a large prediction from f_{θ} indicates that the action \mathbf{a}_t is believed to be optimal for a different state. The prediction units are also directly interpretable.

E. Architecture

Having described the world modeling tasks, we now present the architecture that implements predictors for them.

Networks. Figure 3 shows our setup. We follow [39] and extract observations for each modality – roadgraph, agent locations, traffic lights, and any form of route conditioning – and process them into a unified world state representing the current situation around the ego-vehicle. To capture temporal

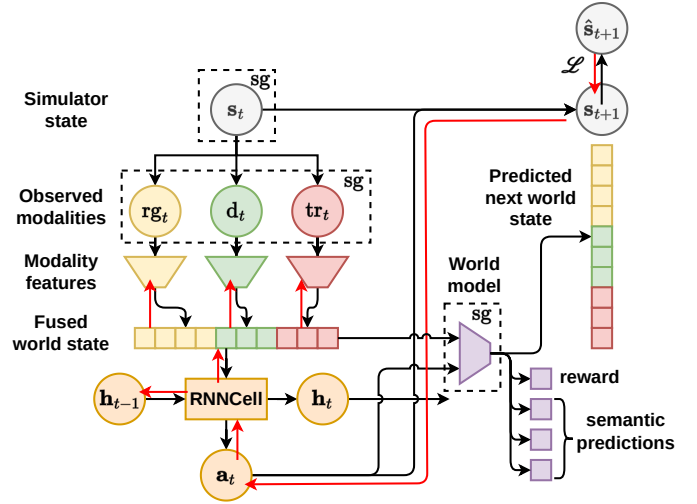


Fig. 3: **Model architecture.** We extract observations for the different modalities (roadgraph rg_t , agent locations d_t , and traffic lights tr_t), process them, and fuse them into a unified latent world state. An RNN evolves the hidden state according to each timestep and selects actions. The world model predicts semantic quantities of interest (purple), allowing for latent imagination and planning. Gradients from the environment dynamics, shown in red, flow through the action execution – we only show for the control task, but in fact similar gradients flow backward also from the world modeling tasks.

information, we use an RNN to evolve a hidden state according to the observed features. A world model with multiple heads predict the next unified world state, a reward, and the estimates for the three tasks introduced previously – relative odometry, state planning, and inverse state estimation.

Losses. We use four main losses – one for the control task, which drives the behavioral policy, and three additional losses for the relative odometry, state planning, and inverse state tasks. Each of these leverages the differentiability of the environment. The inputs to the world model are detached (denoted with $sg[\cdot]$) so the world modeling losses do not impact the behavioral policy. This greatly improves policy stability and makes it so one does not need to weigh the modeling losses relative to the control loss.

For extended functionality, our agent requires three additional auxiliary losses. The first trains the world model to predict the next world state in latent space, which is needed to be able to predict autoregressively arbitrarily long future sequences $\mathbf{z}_t, \mathbf{z}_{t+1}, \dots$. It also allows us to use the AWM task heads on those imagined trajectories, similar to [17, 59]. The second is a reward loss so the world model can predict rewards. We use a standard reward defined as $r_t = -\|\mathbf{s}_{t+1} - \hat{\mathbf{s}}_{t+1}\|_2$. The third loss is an object collision loss, which is sparse and penalizes the ego-vehicle from colliding with other agents. It is described in Sec. III-G

F. Planning at test time

Compared to the APG method in [39], our world modeling predictors enable planning at test time. The relevant workflow

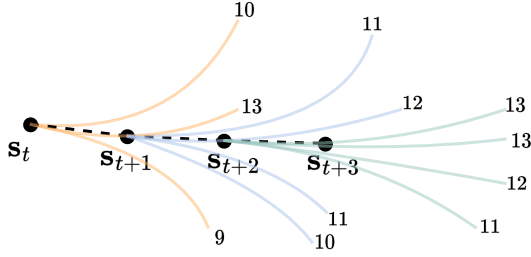


Fig. 4: **Planning.** In each step, planning consists of simulating a few trajectories using the world model (shown here as light orange, purple and green lines), evaluating them (shown as the numbers attached to them), and selecting an aggregated action from the best ones. The actual executed trajectory is shown in dashed black points.

is shown in Fig. 4. Specifically, we adopt a model-predictive control (MPC) algorithm where we first repeatedly compose the world models and the policy to simulate N future trajectories branching out from the current state s_t . Subsequently, the reward model evaluates them and the rewards along each one are summed to yield a single scalar, representing the value of this trajectory. Finally, we select the top- k trajectories in terms of value, and average their first actions. This aggregate action is the one to be executed by the agent at the current step. The planning loop is repeated at every timestep, leading to adaptive, closed loop behavior.

Since the architecture relies on a recurrent model to process the incoming observations, we adapt the planning algorithm to evolve the RNN hidden state within the imagined trajectories. The pseudocode is shown in Algorithm 1.

Algorithm 1 RNN-based MPC planning

Given: $s_t, \mathbf{h}_{t-1}, N_{\text{sim}}$

- 1: Initialize trajectory buffer \mathcal{B}
 - 2: Observe \mathbf{o}_t from s_t
 - 3: $\mathbf{g}_t = \text{FeatureExtractor}(\mathbf{o}_t)$
 - 4: $\mathbf{h}_t = \text{RNN}(\mathbf{g}_t, \mathbf{h}_{t-1})$
 - 5: **for** $i < N_{\text{sim}}$ **do**
 - 6: $\tilde{\mathbf{g}}_\tau, \tilde{\mathbf{h}}_\tau = \mathbf{g}_t, \mathbf{h}_t$
 - 7: **while** simulate with timestep $\tau = \{0, 1, \dots\}$, **do**
 - 8: $\tilde{\mathbf{a}}_\tau^i \sim \text{Actor}(\tilde{\mathbf{g}}_\tau, \tilde{\mathbf{h}}_\tau)$
 - 9: $\tilde{\mathbf{r}}_\tau^i, \tilde{\mathbf{g}}_{\tau+1} = \text{WorldModel}(\tilde{\mathbf{g}}_\tau, \tilde{\mathbf{a}}_\tau^i)$
 - 10: $\tilde{\mathbf{h}}_{\tau+1} = \text{RNN}(\tilde{\mathbf{g}}_{\tau+1}, \tilde{\mathbf{h}}_\tau)$
 - 11: Store $(\tilde{\mathbf{a}}_\tau^i, \tilde{\mathbf{r}}_\tau^i)$ in \mathcal{B}
 - 12: **end while**
 - 13: **end for**
 - 14: Best trajectory $k = \text{argmax}_i \sum_\tau \tilde{\mathbf{r}}_\tau^i$
 - 15: Select $\tilde{\mathbf{a}}_0^k$ for execution
-

Aux. notation: $\mathbf{h}_t = \text{RNN state}$, $\mathbf{g}_t = \text{latent sensory features}$

G. Additional improvements

We have now explained the world modeling tasks, the agent architecture, and the planning. Here we focus on additional practical improvements relevant to our experiments.

Policy generalization. Compared to the APG model in [39], our strategy is to improve the generalization capability of the agent by increasing the diversity of the sampled trajectories. To that end, we first limit the number of training epochs to reduce any possible overfitting, and second, we explicitly add entropy regularization on the actions sampled from the policy [16]. Since the distribution of the actions – steering and acceleration – is modeled as a Gaussian mixture (GM), this regularization is added only for the mixing distribution, which is categorical. To prevent the individual Gaussian distributions from degenerating into deterministic values, we clip their variances to a minimal value.

Differentiable overlap. Being able to detect collisions in Waymax [14] is of crucial importance. The default algorithm there is based on the separation axis theorem and only tells us *whether* two objects overlap, without telling us *how much* they overlap. We are interested in obtaining a differentiable approximation for the overlap between two rotated 2D boxes, so that we can differentiate not only through the dynamics, but also through the scene configuration itself.

We approximate box overlap as the overlap of 2D Gaussians. Specifically, from a vehicle pose (x, y, θ, w, h) , we build a 2D Gaussian with parameters $\boldsymbol{\mu}$ and $\boldsymbol{\Sigma}$ given by:

$$\boldsymbol{\mu} = [x \quad y]^\top \quad (6)$$

$$\boldsymbol{\Sigma} = \mathbf{R} \begin{bmatrix} w^2/25 & 0 \\ 0 & h^2/25 \end{bmatrix} \mathbf{R}^\top \quad (7)$$

$$\mathbf{R} = \begin{bmatrix} \cos \theta & -\sin \theta \\ \sin \theta & \cos \theta \end{bmatrix}. \quad (8)$$

The division by 25 ensures that the density of the Gaussian covers the box relatively well. Then, the overlap between two boxes $\mathcal{N}(\boldsymbol{\mu}_1, \boldsymbol{\Sigma}_1)$ and $\mathcal{N}(\boldsymbol{\mu}_2, \boldsymbol{\Sigma}_2)$ is computed in closed form as another Gaussian density:

$$\frac{1}{2\pi\sqrt{\det(\boldsymbol{\Sigma}_1 + \boldsymbol{\Sigma}_2)}} e^{-\frac{1}{2}(\boldsymbol{\mu}_1 - \boldsymbol{\mu}_2)^\top (\boldsymbol{\Sigma}_1 + \boldsymbol{\Sigma}_2)^{-1} (\boldsymbol{\mu}_1 - \boldsymbol{\mu}_2)}. \quad (9)$$

This overlap provides a very sparse training signal, as the ego-vehicle does not collide all the time. Yet, we include it to make the setup complete in terms of differentiating through both the dynamics and the agent interactions.

IV. EXPERIMENTS

Setup. We follow the settings of [39]. We use the Waymax simulator, whose initial simulator states are built over the WOMD [11]. We measure the quality of a simulated trajectory using the average displacement error (ADE) compared to the expert (log) one. Since the policy is stochastic, we realize multiple trajectories and report the ADE of the best one, leading to minADE. We also report the minimum overlap rate, which represents collisions, and the minimum offroad rate, which represents agents navigating beyond the drivable regions. These rates represent the proportion of scenarios, in which at least one collision/offroad event occurs. All the following results are on the WOMD validation set.

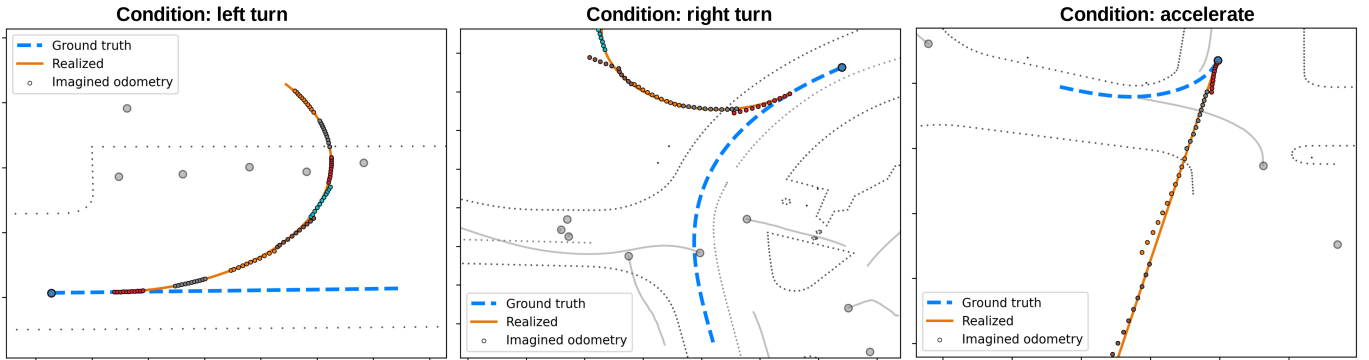


Fig. 5: **Predictions from the next state predictor.** We condition the agent to turn or accelerate. The imagined trajectories, shown as scattered colored circles, represent the imagined odometry of the ego-vehicle in the next 1 second, at different points in time. They align with the actual realized trajectory, which implies that the agent can imagine its motion accurately.

A. Evaluating the analytic predictors

Here we present independent, isolated evaluations for each of the four tasks described in Sec. III.

Optimal control. Optimal control in a differentiable environment can be solved using APG. Hence, we evaluate the reactive performance of our policies similarly to how it was evaluated in the baseline APG method [39]. Table I shows the details. Naturally, the trajectories obtained from rolling out a reactive policy trained with APG are accurate. Increasing the number of rollouts improves performance in terms of min ADE, min overlap, and min offroad by up to 12%.

APG setup	Num. rollouts	min ADE ↓	min overlap ↓	min offroad ↓
APG [39]	32	2.0083	0.0800	0.0282
APG (ours)	1	1.8121	0.0669	0.0263
APG (ours)	2	1.7923	0.0663	0.0257
APG (ours)	4	1.7765	0.0658	0.0256
APG (ours)	8	1.7629	0.0653	0.0252
APG (ours)	16	1.7516	0.0651	0.0251
APG (ours)	32	1.7416	0.0648	0.0248

TABLE I: **APG reactive performance.** Compared to the baseline, we rely on a more efficient training procedure which improves performance by 9% while having 32 times less compute. With equal compute, our method is 12% better in terms of min ADE. Inference time per rollout is similar to the baseline.

Compared to the baseline [39], we use a more efficient training strategy that trains for a smaller number of epochs to limit possible overfitting. Additionally, we aim to increase the diversity of the policy as follows. As previously state, the policy parametrizes a Gaussian mixture with 6 components. We add a regularization term that maximizes the categorical entropy of the mixture distribution (*not* the Gaussians themselves). To prevent the Gaussians from degenerating into single values, we clip the predicted variances.

Relative odometry. To evaluate the next state prediction we first produce qualitative results that demonstrate the controllability of the learned odometry predictor. Specifically, we

condition the agent, for example, to intentionally commit to a turn over a long time frame. Concurrently, the odometry, along with the latent state predictors are used to imagine the next second of the planned motion, conditional on the actions. We judge the imagined trajectory to be accurate if the imagination precisely aligns with the realized trajectory. Fig. 5 shows an example. Overall, we observe accurate controllability – if we condition the agent to turn left/right, accelerate/decelerate, the imagined trajectories also represent similar motion.

Manually conditioning the predicted odometry on a desired action sequence could easily lead to out-of-distribution state-action sequences. For example, driving offroad, making sudden sharp U-turns, or maximally accelerating can be considered rare events within the expert distribution. The accurate alignment between the imagined trajectory and the executed one shows that the network learns to generalize effectively. Nonetheless, the complexity of the scene and the autoregressive prediction length do limit the accuracy of the imagined trajectories. Finally, for in-distribution sequences and for shorter future horizons the odometry is very accurate, as shown in Table II.

Future horizon (steps)	Avg. displacement error ↓
5 (0.5 sec)	0.1698
10 (1 sec)	0.3475
15 (1.5 sec)	0.5496

TABLE II: **Odometry accuracy vs time horizon.** We measure the average distance between the imagined trajectory (of variable length) and the simulated trajectory.

Setting	min ADE ↓	min overlap ↓	min offroad ↓
APG [39]	2.0083	0.0800	0.0282
Planner, Sec. III-C	1.8734	0.0719	0.0254

TABLE III: **Reactive evaluation of the planner.** A differentiable simulator allows us to train a planner with strong performance. Here the planner is deterministic.

Optimal planners. Here we evaluate with a combination of

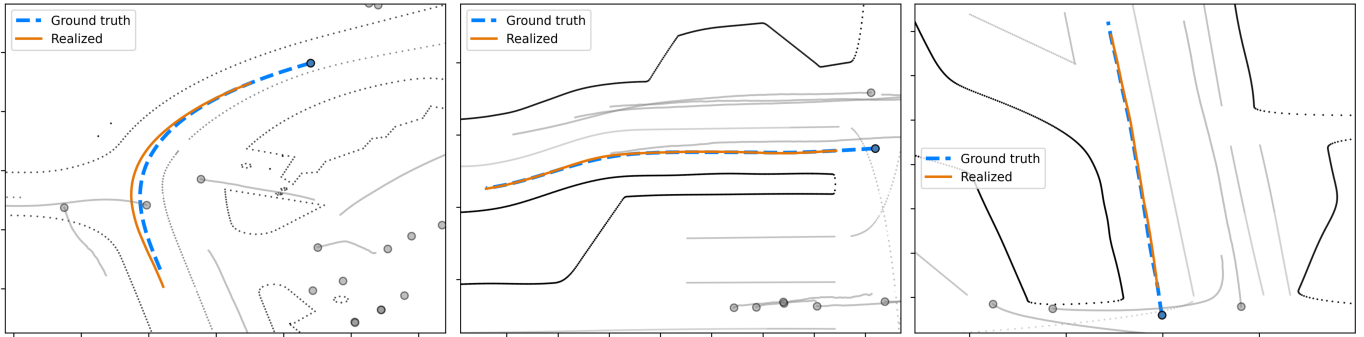


Fig. 6: **Trajectories executed using the optimal planner.** They are realistic and resemble those from the policy. Training such planners is possible due to the analytically available dynamics and inverse kinematics.

quantitative and qualitative metrics. Table III shows that obtaining an optimal planner using a differentiable environment is possible and results in strong performance, improving over the baseline APG method [39] on all metrics. For simplicity, the planner is deterministic. During the training, we found it useful to disable the action clipping that is used by default in the inverse dynamics, as it prevents gradients from flowing backward and updating the planner. This is needed especially early on in the training when the planner network is not accurate and the resulting actions are too large in magnitude. At test time, we evaluate with the default dynamics where action clipping is enabled.

Fig. 6 shows how the trajectories look qualitatively. Overall, they are smooth and realistic. Errors occur mostly from over-accelerating. Some turns are sharper but still reasonable.

Inverse optimal state prediction. Finding a state in which a given action is optimal is an inverse task. To motivate the setup for its evaluation, we reason as follows. If we start from a log state \hat{s}_t and the selected action is optimal, \hat{a}_t , then the state we are looking for has a displacement of exactly $\mathbf{0}$ from the given state \hat{s}_t . Thus, if we assume that the given actions are similar to the expert ones, then the predicted displacement should indicate how far the ego-vehicle is from the current log state \hat{s}_t . This allows us, for example, to take the negative norm of the predicted displacement, $-\|f_\theta(s_t, a_t)\|$, and use it as a confidence-based reward when planning. Table IV shows the performance of this setup. A trained policy is assumed to be near-optimal, hence the predicted inverse state displacements can serve as a reward/uncertainty measure for how close the agent is to where it should be.

We also provide qualitative evaluation in Fig. 7. The results are generally meaningful – as the agent drifts off from the log trajectory, for example by lagging behind it, the predicted inverse optimal state has larger displacement relative to the current state.

B. Planning

Next, we assess the performance of the planning agent, which uses the analytic predictors. Evaluating with the best of multiple trajectory realizations is common practice in the literature [11, 36, 3], yet is unrealistic because in the real world the agent can execute only one trajectory. Planning at test time

Rewards	min ADE ↓	min overlap* ↓	min offroad* ↓
Neg. dist. to next log state	1.8136	0.0645	0.0226
Pos. dist. to next log state	1.8247	0.0649	0.0229
Neg. norm. of inv. state	1.8138	0.0647	0.0218

TABLE IV: **Using the inverse state predictions when planning.** Using the negative norm of the inverse state displacement as reward provides meaningful and strong results. It is only marginally less accurate than using the standard rewards, defined as the negative distance to the next log state, due to the actions not being perfectly optimal. The case of selecting the worst reward (pos. dist to next log state) is also included for reference.

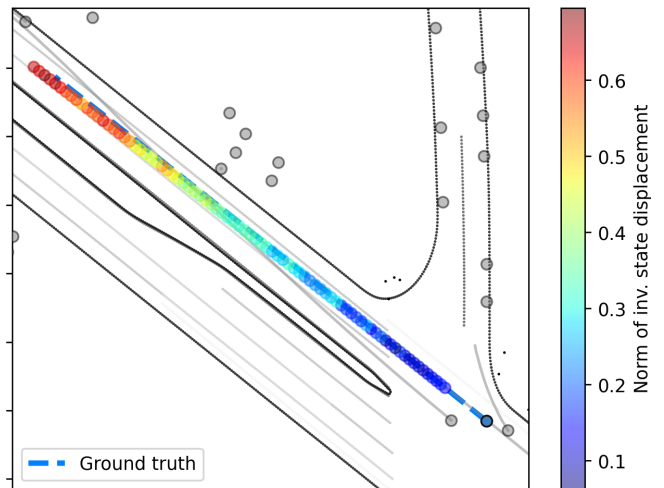


Fig. 7: **Executed trajectory colored according to the norm of the predicted inverse state displacements.** Here, since the ego-vehicle drives slower than the log expert, the norm of the optimal inverse state predictions gradually increases.

is a considerable improvement to this setup because it allows the agent to simulate multiple virtual trajectories while only executing a single real one.

Table V shows results when planning. We increase the number of imagined trajectories while keeping the length of each one constant and equal to one step in the future.

This is because the path with minimum ADE on the whole trajectory contains the path of minimum ADE on any part of the trajectory, allowing one to be greedy and to choose actions only based on their immediate effects. Increasing the number of imagined trajectories from which to aggregate the selected action improves performance. The effect is small but visible. It is small because the variance of the action distribution is small and the agent is confident. Hence, the different considered actions are also similar. Yet, the reward signal is precise enough to allow for the selection of the best ones.

Setting	Num. rollouts	min ADE ↓	min overlap* ↓	min offroad* ↓
Plan + heading	1	1.8147	0.0645	0.0222
Plan + heading	4	1.8121	0.0642	0.0220
Plan + heading	8	1.8113	0.0643	0.0224
Plan + waypoint	1	0.6031	0.0110	0.0098
Plan + waypoint	6	0.5988	0.0107	0.0092
Plan + waypoint	12	0.5980	0.0106	0.0092

TABLE V: **Planning at test time using MPC.** As the number of imagined trajectories increases, performance improves. We condition on either the heading or the last expert waypoint. Effects are limited by the policy diversity, yet are noticeable.

C. Additional experiments

Route conditioning. To obtain good performance in terms of ADE the agent needs to know both where to go, and how to get there. Route conditioning can be used to provide more information to the agent, effectively narrowing down the possible directions that could be taken. We explore two forms of route conditioning – heading, where the agent receives the heading angle to keep in order to reach a future expert state, and waypoint, where the agent observes the (x, y) location of the last expert state. Both are used in the ego reference frame.

Table VI shows that adding route conditioning helps noticeably. Using the waypoint is the most useful because to reach the expert location, the agent needs to adapt both its steering and acceleration. The heading conditioning only provides information about the steering, not the acceleration. In general, as more conditioning is added, the task becomes closer and closer to trajectory following. The heading conditioning is the default setting we use in the other experiments.

Differentiable overlap. We also provide experiments related to the differentiable overlap approximation used by our method. Table VII shows that the differentiable overlap has a small effect – it hurts the ADE, but improves the overlap metric. The differentiable overlap loss pushes the agent in the direction of maximally decreasing overlap when there is a collision. This direction may be different than the one towards the expert state (see Fig. 8). Thus, we recognize a trade-off. To limit the effect of conflicting gradients, we set the weight of the differentiable loss term to a small number.

Conditioning	Num. rollouts	min ADE ↓	min overlap ↓	min offroad ↓
None	1	2.3244	0.1150	0.0774
	8	2.2349	0.1103	0.0738
Heading	1	1.7463	0.0609	0.0234
	8	1.6718	0.0579	0.0222
Last waypoint	1	0.6029	0.0110	0.0098
	8	0.5736	0.0108	0.0094
Wayformer	1	2.3800	0.1068	0.0789

TABLE VI: **Performance of the reactive policy with different levels of conditioning.** Adding more path conditioning improves performance because the policy does not need to decide where to go, only how to get there. For simplicity, we evaluate only the reactive policies. The Wayformer [40] from [14] uses Delta dynamics (not bicycle) and is unconditioned. It is added for reference.

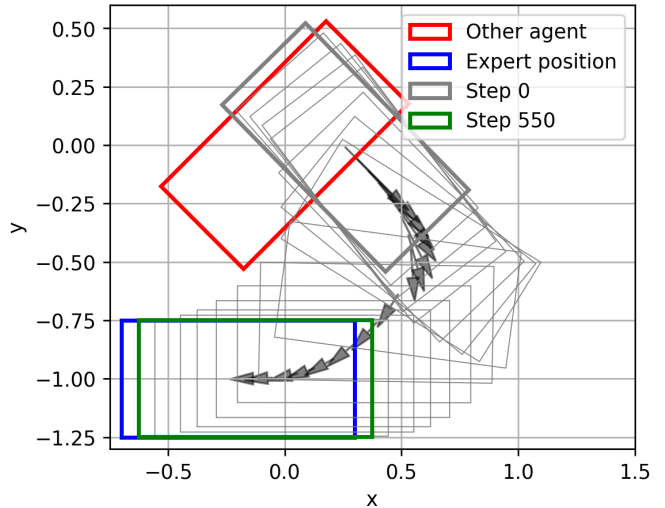


Fig. 8: **Optimizing differentiable overlap.** Here we use two losses – an overlap loss to push the gray box away from the red box and a trajectory loss to pull the gray box toward the blue one. The gradients from these losses point in different directions at every step, leading to a curved trajectory.

D. Implementation details

Training details. We use Adam for the optimizer and a cosine schedule for the learning rate. Training lasts 40 epochs and is done on 8 A100 GPUs, with a total batch size of 256 samples. Each sample here refers to a full WOMD scenario of length 9 seconds. The agent is lightweight with 6M parameters altogether, similar to other models working over intermediate-level traffic scenario representations [36] (roadgraph, 2D boxes). Inference speed is almost 23K timesteps processed per second on a single GPU. Further details, including how the prediction tasks are formulated for the specific dynamics in Waymax [14], are available in the supplementary materials.

V. LIMITATIONS

While our setup yields strong results, it has limitations.

Camera tokens. Raw camera images are unavailable in WOMD [11]. Recently however, camera token features have

Differentiable collision loss	Num. rollouts	min ADE ↓	min overlap* ↓	min offroad* ↓
✗	1	1.7992	0.0146	0.0056
	8	1.7261	0.0141	0.0056
✓	1	1.8186	0.0139	0.0057
	8	1.7456	0.0131	0.0055

TABLE VII: **Adding differentiable overlap.** Adding a small differentiable overlap loss term hurts the ADE metric, but optimizes the overlap. The effect is small because the collision signal is sparse and its loss weight is small. Here, overlap* and offroad* denote that the metric has been calculated as a percentage of all individual *steps*, not *trajectories*, to better show small changes.

been released [37]. They are obtained from a custom pretrained VIT-VQGAN [63]. While they are not ideal, we recognize their potential utility in providing high-quality semantic information. Processing them is usually done with a separate transformer [9, 56], increasing computational cost and memory usage, which we decided to avoid here.

Policy gradient improvements. Despite using differentiable simulation, our APG approach follows the vanilla REINFORCE algorithm in style. It does not use importance-sampling for off-policy correction or rollout buffers for storing previous trajectories. Each batch of collected trajectories is used to update the policy only once, after which it is discarded. Techniques similar to PPO [49] and TRPO [48] could be added to improve stability and data reuse.

Multi-modal policy. In most experiments where we do not use categorical entropy regularization, the Gaussian mixture usually degenerates to a single Gaussian that is selected with 99% probability as training progresses. We view this as expected, given that there is only one expert trajectory per scenario, yet we recognize that more work is needed to maintain a multimodal stochastic policy.

VI. CONCLUSION

In this work, we presented Analytic World Models (AWMs) – different forms of learning world dynamics within a differentiable simulator. We formulated tasks for realtive odometry, optimal planning, and inverse optimal state estimation, all relying on the white box nature of the environment dynamics. We implemented predictors for these tasks within an autonomous vehicle navigation setting. When combined with MPC planning, the world modeling predictors can be used to better gauge the knowledge of the agent and inspect its decisions in a more understandable manner. Additionally, through a better training recipe, our model significantly outperforms the previous APG baseline, obtaining up to 12% lower average displacement error with no increase in compute cost when used in a reactive manner.

VII. ACKNOWLEDGMENTS

This research was partially funded by the Ministry of Education and Science of Bulgaria (support for INSAIT, part of the Bulgarian National Roadmap for Research Infrastructure).

REFERENCES

- [1] Javier Arroyo, Carlo Manna, Fred Spiessens, and Lieve Helsen. Reinforced model predictive control (rl-mpc) for building energy management. *Applied Energy*, 309: 118346, 2022.
- [2] Dimitri Bertsekas. *Dynamic programming and optimal control: Volume I*, volume 4. Athena scientific, 2012.
- [3] Holger Caesar, Varun Bankiti, Alex H Lang, Sourabh Vora, Venice Erin Liong, Qiang Xu, Anush Krishnan, Yu Pan, Giancarlo Baldan, and Oscar Beijbom. nuscenes: A multimodal dataset for autonomous driving. In *Proceedings of the IEEE/CVF conference on computer vision and pattern recognition*, pages 11621–11631, 2020.
- [4] Sirui Chen, Yunhao Liu, Shang Wen Yao, Jialong Li, Tingxiang Fan, and Jia Pan. Diffssl: Learning dynamical state representation for deformable object manipulation with differentiable simulation. *IEEE Robotics and Automation Letters*, 7(4):9533–9540, 2022.
- [5] Kurtland Chua, Roberto Calandra, Rowan McAllister, and Sergey Levine. Deep reinforcement learning in a handful of trials using probabilistic dynamics models. *Advances in neural information processing systems*, 31, 2018.
- [6] Felipe Codevilla, Matthias Müller, Antonio López, Vladlen Koltun, and Alexey Dosovitskiy. End-to-end driving via conditional imitation learning. In *2018 IEEE international conference on robotics and automation (ICRA)*, pages 4693–4700. IEEE, 2018.
- [7] Filipe de Avila Belbute-Peres, Kevin Smith, Kelsey Allen, Josh Tenenbaum, and J Zico Kolter. End-to-end differentiable physics for learning and control. *Advances in neural information processing systems*, 31, 2018.
- [8] Jonas Degraeve, Michiel Hermans, Joni Dambre, and Francis Wyffels. A differentiable physics engine for deep learning in robotics. *Frontiers in neurorobotics*, 13:6, 2019.
- [9] Alexey Dosovitskiy. An image is worth 16x16 words: Transformers for image recognition at scale. *arXiv preprint arXiv:2010.11929*, 2020.
- [10] Alexey Dosovitskiy, German Ros, Felipe Codevilla, Antonio Lopez, and Vladlen Koltun. Carla: An open urban driving simulator. In *Conference on robot learning*, pages 1–16. PMLR, 2017.
- [11] Scott Ettinger, Shuyang Cheng, Benjamin Caine, Chenxi Liu, Hang Zhao, Sabeek Pradhan, Yuning Chai, Ben Sapp, Charles R Qi, Yin Zhou, et al. Large scale interactive motion forecasting for autonomous driving: The waymo open motion dataset. In *Proceedings of the IEEE/CVF International Conference on Computer Vision*, pages 9710–9719, 2021.
- [12] C Daniel Freeman, Erik Frey, Anton Raichuk, Sertan Girgin, Igor Mordatch, and Olivier Bachem. Brax—a differentiable physics engine for large scale rigid body simulation. *arXiv preprint arXiv:2106.13281*, 2021.
- [13] Moritz Geilinger, David Hahn, Jonas Zehnder, Moritz

- Bächer, Bernhard Thomaszewski, and Stelian Coros. Add: Analytically differentiable dynamics for multi-body systems with frictional contact. *ACM Transactions on Graphics (TOG)*, 39(6):1–15, 2020.
- [14] Cole Gulino, Justin Fu, Wenjie Luo, George Tucker, Eli Bronstein, Yiren Lu, Jean Harb, Xinlei Pan, Yan Wang, Xiangyu Chen, et al. Waymax: An accelerated, data-driven simulator for large-scale autonomous driving research. *Advances in Neural Information Processing Systems*, 36, 2024.
- [15] David Ha and Jürgen Schmidhuber. World models. *arXiv preprint arXiv:1803.10122*, 2018.
- [16] Tuomas Haarnoja, Aurick Zhou, Pieter Abbeel, and Sergey Levine. Soft actor-critic: Off-policy maximum entropy deep reinforcement learning with a stochastic actor. In *International conference on machine learning*, pages 1861–1870. PMLR, 2018.
- [17] Danijar Hafner, Timothy Lillicrap, Jimmy Ba, and Mohammad Norouzi. Dream to control: Learning behaviors by latent imagination. *arXiv preprint arXiv:1912.01603*, 2019.
- [18] Danijar Hafner, Timothy Lillicrap, Mohammad Norouzi, and Jimmy Ba. Mastering atari with discrete world models. *arXiv preprint arXiv:2010.02193*, 2020.
- [19] Danijar Hafner, Jurgis Pasukonis, Jimmy Ba, and Timothy Lillicrap. Mastering diverse domains through world models. *arXiv preprint arXiv:2301.04104*, 2023.
- [20] Johannes Heeg, Yunlong Song, and Davide Scaramuzza. Learning quadrotor control from visual features using differentiable simulation. *arXiv preprint arXiv:2410.15979*, 2024.
- [21] Eric Heiden, Miles Macklin, Yashraj Narang, Dieter Fox, Animesh Garg, and Fabio Ramos. Disect: A differentiable simulation engine for autonomous robotic cutting. *arXiv preprint arXiv:2105.12244*, 2021.
- [22] Philipp Holl, Vladlen Koltun, and Nils Thuerey. Learning to control pdes with differentiable physics. *arXiv preprint arXiv:2001.07457*, 2020.
- [23] Yuanming Hu, Luke Anderson, Tzu-Mao Li, Qi Sun, Nathan Carr, Jonathan Ragan-Kelley, and Frédo Durand. DiffTaichi: Differentiable programming for physical simulation. *arXiv preprint arXiv:1910.00935*, 2019.
- [24] Wenzel Jakob, Sébastien Speierer, Nicolas Roussel, and Delio Vicini. Dr. jit: A just-in-time compiler for differentiable rendering. *ACM Transactions on Graphics (TOG)*, 41(4):1–19, 2022.
- [25] Napat Karnchanachari, Miguel Iglesia Valls, David Hoeller, and Marco Hutter. Practical reinforcement learning for mpc: Learning from sparse objectives in under an hour on a real robot. In *Learning for Dynamics and Control*, pages 211–224. PMLR, 2020.
- [26] Samuli Laine, Janne Hellsten, Tero Karras, Yeongho Seol, Jaakko Lehtinen, and Timo Aila. Modular primitives for high-performance differentiable rendering. *ACM Transactions on Graphics (ToG)*, 39(6):1–14, 2020.
- [27] Jonathan Wilder Lavington, Ke Zhang, Vasileios Lioutas, Matthew Niedoba, Yunpeng Liu, Dylan Green, Saeid Naderiparizi, Xiaoxuan Liang, Setareh Dabiri, Adam Ścibior, et al. Torchdriveenv: A reinforcement learning benchmark for autonomous driving with reactive, realistic, and diverse non-playable characters. *arXiv preprint arXiv:2405.04491*, 2024.
- [28] Quanyi Li, Zhenghao Peng, Lan Feng, Qihang Zhang, Zhenghai Xue, and Bolei Zhou. Metadrive: Composing diverse driving scenarios for generalizable reinforcement learning. *IEEE transactions on pattern analysis and machine intelligence*, 45(3):3461–3475, 2022.
- [29] Sizhe Li, Zhiao Huang, Tao Chen, Tao Du, Hao Su, Joshua B Tenenbaum, and Chuang Gan. Dexdeform: Dexterous deformable object manipulation with human demonstrations and differentiable physics. *arXiv preprint arXiv:2304.03223*, 2023.
- [30] Xingyu Lin, Zhiao Huang, Yunzhu Li, Joshua B Tenenbaum, David Held, and Chuang Gan. Diffskill: Skill abstraction from differentiable physics for deformable object manipulations with tools. *arXiv preprint arXiv:2203.17275*, 2022.
- [31] Björn List, Li-Wei Chen, and Nils Thuerey. Learned turbulence modelling with differentiable fluid solvers: physics-based loss functions and optimisation horizons. *Journal of Fluid Mechanics*, 949:A25, 2022.
- [32] Michael Lutter, Johannes Silberbauer, Joe Watson, and Jan Peters. Differentiable physics models for real-world offline model-based reinforcement learning. In *2021 IEEE International Conference on Robotics and Automation (ICRA)*, pages 4163–4170. IEEE, 2021.
- [33] Miles Macklin. Warp: A high-performance python framework for gpu simulation and graphics. <https://github.com/nvidia/warp>, March 2022. NVIDIA GPU Technology Conference (GTC).
- [34] Mark Martinez, Chawin Sitawarin, Kevin Finch, Lennart Meincke, Alex Yablonski, and Alain Kornhauser. Beyond grand theft auto v for training, testing and enhancing deep learning in self driving cars. *arXiv preprint arXiv:1712.01397*, 2017.
- [35] Thomas M Moerland, Joost Broekens, Aske Plaat, Catholijn M Jonker, et al. Model-based reinforcement learning: A survey. *Foundations and Trends® in Machine Learning*, 16(1):1–118, 2023.
- [36] Nico Montali, John Lambert, Paul Mougins, Alex Kuefler, Nicholas Rhinehart, Michelle Li, Cole Gulino, Tristan Emrich, Zoey Yang, Shimon Whiteson, et al. The waymo open sim agents challenge. *Advances in Neural Information Processing Systems*, 36, 2024.
- [37] Norman Mu, Jingwei Ji, Zhenpei Yang, Nate Harada, Haotian Tang, Kan Chen, Charles R Qi, Runzhou Ge, Kratarth Goel, Zoey Yang, et al. Most: Multi-modality scene tokenization for motion prediction. In *Proceedings of the IEEE/CVF Conference on Computer Vision and Pattern Recognition*, pages 14988–14999, 2024.
- [38] J Krishna Murthy, Miles Macklin, Florian Golemo, Vikram Voleti, Linda Petrini, Martin Weiss, Brendan

- Considine, Jérôme Parent-Lévesque, Kevin Xie, Kenny Erleben, et al. grdsim: Differentiable simulation for system identification and visuomotor control. In *International conference on learning representations*, 2020.
- [39] Asen Nachkov, Danda Pani Paudel, and Luc Van Gool. Autonomous vehicle controllers from end-to-end differentiable simulation. *arXiv preprint arXiv:2409.07965*, 2024.
- [40] Nigamaa Nayakanti, Rami Al-Rfou, Aurick Zhou, Kratarth Goel, Khaled S Refaat, and Benjamin Sapp. Wayformer: Motion forecasting via simple & efficient attention networks. In *2023 IEEE International Conference on Robotics and Automation (ICRA)*, pages 2980–2987. IEEE, 2023.
- [41] Rhys Newbury, Jack Collins, Kerry He, Jiahe Pan, Ingmar Posner, David Howard, and Akansel Cosgun. A review of differentiable simulators. *IEEE Access*, 2024.
- [42] Chris J Ostafew, Angela P Schoellig, and Timothy D Barfoot. Robust constrained learning-based nmppc enabling reliable mobile robot path tracking. *The International Journal of Robotics Research*, 35(13):1547–1563, 2016.
- [43] Deepak Pathak, Pulkit Agrawal, Alexei A Efros, and Trevor Darrell. Curiosity-driven exploration by self-supervised prediction. In *International conference on machine learning*, pages 2778–2787. PMLR, 2017.
- [44] Athanasios S Polydoros and Lazaros Nalpantidis. Survey of model-based reinforcement learning: Applications on robotics. *Journal of Intelligent & Robotic Systems*, 86(2):153–173, 2017.
- [45] Yi-Ling Qiao, Junbang Liang, Vladlen Koltun, and Ming C Lin. Scalable differentiable physics for learning and control. *arXiv preprint arXiv:2007.02168*, 2020.
- [46] Angel Romero, Yunlong Song, and Davide Scaramuzza. Actor-critic model predictive control. In *2024 IEEE International Conference on Robotics and Automation (ICRA)*, pages 14777–14784. IEEE, 2024.
- [47] Julian Schrittwieser, Ioannis Antonoglou, Thomas Hubert, Karen Simonyan, Laurent Sifre, Simon Schmitt, Arthur Guez, Edward Lockhart, Demis Hassabis, Thore Graepel, et al. Mastering atari, go, chess and shogi by planning with a learned model. *Nature*, 588(7839):604–609, 2020.
- [48] John Schulman, Sergey Levine, Pieter Abbeel, Michael Jordan, and Philipp Moritz. Trust region policy optimization. In *International conference on machine learning*, pages 1889–1897. PMLR, 2015.
- [49] John Schulman, Filip Wolski, Prafulla Dhariwal, Alec Radford, and Oleg Klimov. Proximal policy optimization algorithms. *arXiv preprint arXiv:1707.06347*, 2017.
- [50] Zilin Si, Gu Zhang, Qingwei Ben, Branden Romero, Zhou Xian, Chao Liu, and Chuang Gan. Diff tactile: A physics-based differentiable tactile simulator for contact-rich robotic manipulation. *arXiv preprint arXiv:2403.08716*, 2024.
- [51] Yunlong Song, Sangbae Kim, and Davide Scaramuzza. Learning quadruped locomotion using differentiable simulation. *arXiv preprint arXiv:2403.14864*, 2024.
- [52] Qiao Sun, Xin Huang, Brian C Williams, and Hang Zhao. Intersim: Interactive traffic simulation via explicit relation modeling. in 2022 ieeee. In *RSJ International Conference on Intelligent Robots and Systems (IROS)*, pages 11416–11423, 2022.
- [53] Richard S Sutton. Dyna, an integrated architecture for learning, planning, and reacting. *ACM Sigart Bulletin*, 2(4):160–163, 1991.
- [54] Marc A Toussaint, Kelsey Rebecca Allen, Kevin A Smith, and Joshua B Tenenbaum. Differentiable physics and stable modes for tool-use and manipulation planning. 2018.
- [55] Kiwon Um, Robert Brand, Yun Raymond Fei, Philipp Holl, and Nils Thuerey. Solver-in-the-loop: Learning from differentiable physics to interact with iterative pde-solvers. *Advances in Neural Information Processing Systems*, 33:6111–6122, 2020.
- [56] A Vaswani. Attention is all you need. *Advances in Neural Information Processing Systems*, 2017.
- [57] Eugene Vinitzky, Nathan Lichtlé, Xiaomeng Yang, Brandon Amos, and Jakob Foerster. Nocturne: a scalable driving benchmark for bringing multi-agent learning one step closer to the real world. *Advances in Neural Information Processing Systems*, 35:3962–3974, 2022.
- [58] Nina Wiedemann, Valentin Wüest, Antonio Loquercio, Matthias Müller, Dario Floreano, and Davide Scaramuzza. Training efficient controllers via analytic policy gradient. In *2023 IEEE International Conference on Robotics and Automation (ICRA)*, pages 1349–1356. IEEE, 2023.
- [59] Philipp Wu, Alejandro Escontrela, Danijar Hafner, Pieter Abbeel, and Ken Goldberg. Daydreamer: World models for physical robot learning. In *Conference on robot learning*, pages 2226–2240. PMLR, 2023.
- [60] Jie Xu, Tao Chen, Lara Zlokapa, Michael Foshey, Wojciech Matusik, Shinjiro Sueda, and Pulkit Agrawal. An end-to-end differentiable framework for contact-aware robot design. *arXiv preprint arXiv:2107.07501*, 2021.
- [61] Jie Xu, Viktor Makoviychuk, Yashraj Narang, Fabio Ramos, Wojciech Matusik, Animesh Garg, and Miles Macklin. Accelerated policy learning with parallel differentiable simulation. *arXiv preprint arXiv:2204.07137*, 2022.
- [62] Jie Xu, Sangwoon Kim, Tao Chen, Alberto Rodriguez Garcia, Pulkit Agrawal, Wojciech Matusik, and Shinjiro Sueda. Efficient tactile simulation with differentiability for robotic manipulation. In *Conference on Robot Learning*, pages 1488–1498. PMLR, 2023.
- [63] Jiahui Yu, Xin Li, Jing Yu Koh, Han Zhang, Ruoming Pang, James Qin, Alexander Ku, Yuanzhong Xu, Jason Baldridge, and Yonghui Wu. Vector-quantized image modeling with improved vqgan. *arXiv preprint arXiv:2110.04627*, 2021.
- [64] Jingwei Zhang, Lei Tai, Peng Yun, Yufeng Xiong, Ming Liu, Joschka Boedecker, and Wolfram Burgard. Vr-

goggles for robots: Real-to-sim domain adaptation for visual control. *IEEE Robotics and Automation Letters*, 4 (2):1148–1155, 2019.

[65] Shuang Zhao, Wenzel Jakob, and Tzu-Mao Li. Physics-based differentiable rendering: from theory to implementation. In *ACM siggraph 2020 courses*, pages 1–30. 2020.

APPENDIX A IMPLEMENTATION DETAILS

The task formulations presented in Section III are conceptual. We now discuss their concrete formulation in the Waymax simulator [14] for the bicycle dynamics, where the agent predicts acceleration a and steering κ .

Bicycle model. In the bicycle model the agent state is given by (x, y, θ, v_x, v_y) , containing the (x, y) location in global coordinates, the yaw angle θ , and the velocities (v_x, v_y) over the two global axes. The actions $\mathbf{a} = (a, \kappa)$ consist of acceleration and steering. Given an action, the agent state evolves to its new values $(x', y', \theta', v'_x, v'_y)$ as follows:

$$\begin{aligned} x' &= x + v_x \Delta t + \frac{1}{2} a \cos \theta \Delta t^2 \\ y' &= y + v_y \Delta t + \frac{1}{2} a \sin \theta \Delta t^2 \\ \theta' &= \theta + \kappa \left[\sqrt{v_x^2 + v_y^2} \Delta t + \frac{1}{2} a \Delta t^2 \right] \\ v' &= \sqrt{v_x^2 + v_y^2} + a \Delta t \\ v'_x &= v' \cos \theta' \\ v'_y &= v' \sin \theta'. \end{aligned} \quad (10)$$

We study the dynamics by fixing a single transition from a trajectory and exploring the behavior of a predictor being trained with gradient descent to overfit on this transition.

Relative odometry. For the relative odometry task in III-B, one can notice that, while $\mathbf{s}_{t+1} - \mathbf{s}_t$ is a guaranteed optimal, where the loss function attains a value of zero, it is not the only optimal point. Indeed, our results suggest that if the network f_ϕ predicts a full agent state $\tilde{\mathbf{s}}_t = (x, y, \theta, v_x, v_y)$, then there are many states $\tilde{\mathbf{s}}_t$ from which taking an action \mathbf{a}_t will bring us to $\mathbf{s}_{t+1} = (x', y', \theta', v'_x, v'_y)$. Intuitively, if (x, y) is predicted closer to (x', y') , then (v_x, v_y) can also be predicted smaller. Under the fixed action, we do not need a large initial velocity to reach a point that is relatively close. However, what can happen is that (x, y) is predicted to be far from (x', y') , and (v_x, v_y) are also predicted to be large. From a more distant point the agent needs to have a larger initial velocity to reach the target point, under a fixed action $\mathbf{a}_t = (a, \kappa)$.

Empirically, this means that even though gradient descent perfectly minimizes the loss, it may not learn to predict $\mathbf{s}_{t+1} - \mathbf{s}_t$. Since it is useful to have precisely this difference learned by the network, and since at test time it is mostly the (x, y, θ) variables that matter for our planning, we limit our dynamics predictor f_ϕ to predict only $(\Delta x, \Delta y, \Delta \theta)$, and take the velocities to be fixed at their current values in \mathbf{s}_t . This guarantees the prediction convergence to $\mathbf{s}_{t+1} - \mathbf{s}_t$. Yet, we can supervise all five variables (x, y, θ, v_x, v_y) of the simulated

state, because the relative odometry task uses only transitions collected from the behavioral policy.

In brief, the concrete relative odometry task we solve is: given action (a, κ) , predict $(\Delta x, \Delta y, \Delta \theta)$ such that the state $(x_t + \Delta x, y_t + \Delta y, \theta_t + \Delta \theta, v_{x,t}, v_{y,t})$ evolves to $(x_{t+1}, y_{t+1}, \theta_{t+1}, v_{x,t+1}, v_{y,t+1})$. Formulated in this way, there is a unique global minimizer.

Optimal inverse state. The setting is similar for the inverse optimal state estimation, presented in Section III-D. One can either predict the full state (x, y, θ, v_x, v_y) , obtaining one of possibly many solutions, or one can predict only the elements (x, y, θ) , in which case whatever prediction gradient descent converges to will be the unique prediction. We opt for the latter. Our final prediction problem is: given action (a, κ) , predict $(\Delta x, \Delta y, \Delta \theta)$ such that the state $(x_t + \Delta x, y_t + \Delta y, \theta_t + \Delta \theta, v_{x,t}, v_{y,t})$ evolves to $(\hat{x}_{t+1}, \hat{y}_{t+1}, \hat{\theta}_{t+1}, \hat{v}_{x,t+1}, \hat{v}_{y,t+1})$, where the target is, this time, the expert state. We apply the loss only over (x, y) elements because the target combination of $(\hat{x}_{t+1}, \hat{y}_{t+1}, \hat{v}_{x,t+1}, \hat{v}_{y,t+1})$ may be, in general, unreachable from the current state.

Optimal planning. For the optimal planner task in III-C, we study the inverse kinematics equations:

$$\begin{aligned} a &= \left[\sqrt{v_x'^2 + v_y'^2} - \sqrt{v_x^2 + v_y^2} \right] / \Delta t \\ \kappa &= \left(\arctan \frac{v'_x}{v'_y} - \theta \right) / \left[\sqrt{v_x^2 + v_y^2} \Delta t + \frac{1}{2} a \Delta t^2 \right] \end{aligned} \quad (11)$$

Here, it is enough to predict only (v'_x, v'_y) in order to determine the action that brings the agent to the next state. In this setting, we have also found it useful to remove the typical action clipping applied, because in the cases where (v'_x, v'_y) are too large, the action obtained from the inverse kinematics will be clipped, which prevents gradients from flowing back and updating the model weights. To make this task have a unique minimizer for each transition, we predict (v'_x, v'_y) and supervise only the (x, y, θ) elements.

In summary, these tasks require inverting the bicycle dynamics, which depending on the formulation, may not always be one-to-one. We need to condition the prediction on additional variables, so that the minimizers are unique. This requirement stems from the underlying dynamics model itself.

Coordinate systems. Even though we phrase the world modeling tasks using actual simulator states, e.g. $\mathbf{s}_t, \mathbf{a} \mapsto \mathbf{s}_{t+1}$, the precise inputs to our world modeling predictors f_θ are always in the local time-dependent ego-vehicle reference frame. Additionally, one needs to take care to make sure that the state additions and subtractions in Eqns. 3, 4, and 5 are all done in the same coordinate frame.